A Hybrid Catalyst-Bonded Membrane Device for Electrochemical Carbon Monoxide Reduction at Different Relative Humidities

Supporting Information File

Ian Sullivan[1], Lihao Han[1], Soo Hong Lee[2], Meng Lin[1], David M. Larson[2], Walter S. Drisdell[2], and Chengxiang Xiang[1]*

[1] Joint Center for Artificial Photosynthesis, and Division of Chemistry and Chemical Engineering, California Institute of Technology, 1200 E California Blvd. Pasadena, California 91125, United States

[2] Joint Center for Artificial Photosynthesis, and Chemical Sciences Division, Lawrence Berkeley National Lab, 1 Cyclotron Rd. Berkeley, California, 94720 United States

This supporting information file contains 16 pages, 14 figures, and 2 tables.

Cu Electrodeposition

Cu was electrodeposited on GDLs with a microporous layer (29 BC, Ion Power) in an electrolyte containing 0.15 M $CuCl_2 \cdot 2H_2O$ (99.99%, Alfa Aeasar), 1 M HCl (37% ACS Grade, Sigma Aldrich), and 20% ethanol (Koptek, 200 proof). Preferential deposition of Cu on the microporous layer was achieved by applying polyimide tape (Kapton) to the backside of the GDL and immersing in the electrolyte bath. The cell consisted of the GDL as a working electrode, Cu mesh as a counter electrode, and Ag/AgCl (sat. KCl) as a reference electrode. -0.5 V vs. Ag/AgCl was applied until a charge of 4.5 C/cm^2 was passed. After deposition the Cu-GDE was taken out of solution and dipped in deionized water several times to rinse excess electrolyte. After rinsing, the Kapton tape was removed from the backside and the electrode was allowed to dry in air.

Relative Humidity Control

Relative humidity was controlled using two mass flow controllers (MFC), one with a dry stream of CO (0% RH), and one with a fully humidified stream (100% RH) as shown in Figure S2. Relative humidity is the ratio between water partial pressure and the equilibrium partial pressure of water at a given temperature. For example, to achieve a 50% RH stream, 5 sccm of dry CO and 5 sccm fully humidified CO were mixed in a chamber and delivered to the electrochemical cell. To ensure proper RH values were achieved, a RH meter from Digikey was installed in the mixing chamber and constantly monitored the RH.

Electrochemical Measurements

Electrochemical measurements were performed using a Biologic SP-300 model potentiostat. The custom GDE cell consisted of two plates which sandwiched the Cu-GDE, anion exchange membrane (FAA-3-50, Fumatech), and Pt mesh anode and were tightened with external screws. All measurements were performed at room temperature (25 °C) and pressure (1 atm). The GDE cell was allowed to equilibrate at OCV conditions until the OCV measured -1.0 V. EIS measurements were taken at OCV conditions using a range of frequencies of 200 kHz to 0.1 Hz and amplitude of 10 mV. Cell resistance was taken as the Real resistance measured at 8.7 KHz.

CV scans of $K_3(FeCN_6)_3$ (ferrocyanide) were performed in a traditional aqueous electrolyte (50 mM ferrocyanide/0.5 M KCl) using a Pt disc working electrode (2 mm diameter), Pt wire counter electrode, and Ag/AgCl reference electrode. To perform CV scans of ferrocyanide in the GDE configuration an anion exchange membrane (FAA-3-50, Fumatech) was soaked in a 50 mM ferrocyanide/0.5 M KCl solution overnight and used as the separator in the GDE cell. A Pt mesh served as the working electrode, another Pt mesh served as the counter electrode, and Ag/AgCl served as the reference electrode in the anolyte reservoir (see schematic in main text). 0.5 M KCl was used as the electrolyte, and CV scans were performed in the same manner as the aqueous cell.

Product Analysis

Gas products were measured with online gas chromatography (GC, Model 8610C) customized from SRI instruments. A thermal conductivity detector (TCD) was used to detect H_2, while a flame ionization detector (FID) was used to detect CH_4, C_2H_4, and C_2H_6 products. We employ a parallel column configuration using a Molsieve 5A column for H_2, O_2, N_2, and CO separation, while a Haysep 5D column is used to separate CH_4, CO, CO_2, C_2H_4 and C_2H_6. An isothermal

method is used with an oven temperature of 110 °C, TCD temperature 105 °C, FID temperature 100 °C, injection valve 60 °C. Ar carrier gas was set to 20 psi, H_2 methanizer gas set to 20 psi, and air pump set to 5 psi.

Liquid products were analyzed from the anode side of the cell with high performance liquid chromatography (HPLC, Dionex UltiMate 3000). The eluent was 1 mM H_2SO_4 in water with a flow rate of 0.6 ml/min and column pressure of 76 bar. The column was an Aminex HPX 87-H from Biorad, held at 60 °C with an internal heater. The detector was a UV detector set to 250 nm. Injection volume was 10 μL.

Cu-GDE Characterization

Scanning Electron Microscope (SEM, FEI Inc., NOVA NanoSEM 450) with an integrated energy-dispersive X-ray (EDX) spectroscopy was introduced to analyze the morphology and the elemental composition, respectively. Cu-GDEs were adhered to SEM stubs using double sided copper tape. Images were taken using an accelerating voltage of 5 kV and spot size of 3. EDX images were taken with an accelerating voltage of 15 kV and spot size of 5.

X-ray Diffraction

X-ray diffraction (XRD) measurements were taken with a Bruker D8 Discover X-ray diffractometer using Cu Kα radiation (1.54056 Å) in Bragg-Brentano geometry. Diffraction images were collected using a two-dimensional VÅNTEC-500 detector and integrated into one-dimensional patterns using DIFFRAC.SUITE™ EVA software.

Operando X-ray Absorption Data Collection

Operando X-ray absorption spectroscopy (XAS) measurements were conducted at the Stanford Synchrotron Radiation Lightsource (SSRL) on beamline 7-3 (Cu K-edge). The *operando* experiments were performed under CO gas conditions using a GDE cell setup identical to the one used for evaluating CORR, with the sole modification of a polyimide (Kapton) window to allow for X-ray penetration on the vapor side and was positioned at 45° from the incident X-ray. The radiation was tuned by a Si(220) double-crystal monochromator and the intensity of the incident X-rays (I_0) was monitored by an Ar-filled ion chamber in front of the GDE cell. Data were collected as fluorescence excitation spectra at room temperature using a Ge 30 element detector (Canberra). Spectra were recorded on the dry electrodeposited Cu films at first and then with electrolyte flowing at –1.6 V, –1.8, –2.0, and –2.2 vs Ag/AgCl.

Data analysis of Cu K-edge X-ray absorption near edge spectroscopy (XANES) spectra was performed using the Athena software package.[1] Pre-edge and post-edge backgrounds were subtracted from the XAS spectra, and the resulting spectra were normalized by edge height.

Numerical Model for Water-Vapor Transport

Figure 4a shows the calculation domain of the 2D model for water-vapor transport. The anode side was swept with 1M KOH and cathode with humidified CO. The water-vapor transport within the cathode chamber is described by a two-phase flow model solving for separate Darcy equations for gas and liquid phases, separately[2].

$$\nabla \rho_g u_g = q_g,\ u_g = -\frac{k_g}{\mu_g}\nabla p_g \quad \text{(S1)}$$

$$\nabla \rho_l u_l = q_l,\ u_l = -\frac{k_l}{\mu_l}\nabla p_l \quad \text{(S2)}$$

where ρ is the density, u is the velocity, q the mass sources term, p is the pressure, μ is the viscosity, and k is the permeability. The two sets of Darcy equations are linked by the capillary pressure with liquid saturation predicted by Van Genuchten model.[3]

The mass source terms due to phase change phenomena of water evaporation and condensation (q_{pc}) in the cathode chamber is estimated using the Hertz-Knudsen-Langmuir equation.[4]

$$q_{\mathrm{W,d}} = \begin{cases} \gamma_e C_{\mathrm{H_2O}}\left(\chi_{\mathrm{H_2O}} - \chi_{\mathrm{sat}}\right) & if\ \ \chi_{\mathrm{H_2O}} < \chi_{\mathrm{sat}} \\ \gamma_c C_{\mathrm{H_2O}}\left(\chi_{\mathrm{H_2O}} - \chi_{\mathrm{sat}}\right) & if\ \ \chi_{\mathrm{H_2O}} < \chi_{\mathrm{sat}} \end{cases} \quad \text{(S3)}$$

where $\chi_{\mathrm{H_2O}}$ is the molar fraction of vapor, χ_{sat} is the saturation molar fraction of vapor, γ_e and γ_c are the evaporation and condensation rates .[5]

Transport of gaseous species on the cathode side is captured by considering convective and diffusive terms:

$$\nabla \cdot j_i = \nabla \cdot (-D_i \nabla c_i + c_i u_g) \quad \text{(S4)}$$

where D_i is the diffusion coefficient of each species (D_{CO} = 0.2 cm^2/s and D_{H2O}= 0.277 cm^2/s).[2,6]

The constant mass flow rate of 10 sccm of CO with various relative humidity conditions are given as the inlet boundary. For anode inlet, 10 sccm 1 M KOH flow rate is used as the boundary conditions. Outflow boundary condition is considered for all outlets. Other boundaries are considered as non-slip for fluid flow equations. The parameters used in multi-physics simulations are detailed in table S1.

Table S1. Parameters used in simulations

Anode channel thickness	0.5 mm	measured
GDL thickness	270 μm	measured
MPL thickness	30 μm	measured
Membrane thickness	50 μm	measured
Cell length	2 cm	measured
Inlet and outlet length	0.2 cm	measured
GDL porosity	0.625	reference[7]
MPL porosity	0.25	reference[7]
CL porosity	0.38	reference[7]
GDL permeability	1.8×10^{-11} m^2	reference[7]
MPL permeability	3.33×10^{-15} m^2	reference[7]
CL permeability	2×10^{-15} m^2	reference[7]
GDL tortuosity	2	reference[8]
MPL tortuosity	3	reference[8]
CL tortuosity	3	reference[8]

Three mechanisms of the water transport are considered, i.e. diffusion, water electro-osmotic drag, and hydraulic permeation. The diffusion of water in through the AEM is given by:[2]

$$q_{\mathrm{pc}} = -\frac{D_\lambda}{V_{\mathrm{m}}} \nabla \lambda_{\mathrm{W}} \quad \text{(S5)}$$

where $q_{W,d}$ is the mass flux of water transport due to diffusion, D_λ is the diffusion coefficient, V_m is the molar volume of the dry membrane, and λ_w is the water content in the membrane. The water content of membrane surface at the anode side is considered to be at a constant value of 22 assuming a complete wetting due to continuous anolyte circulation.[4] The water content at membrane cathode side is estimated based on relative humidity[4] :

$$\lambda_w = \begin{cases} 0.043 + 17.81\mathrm{RH} - 39.85\mathrm{RH}^2 + 36\mathrm{RH}^3 \; if \; \mathrm{RH} \leq 1 \\ \lambda_w(\mathrm{RH}=1) + \frac{22-\lambda_w(\mathrm{RH}=1)}{2}(\mathrm{RH}-1) \; if \; \mathrm{RH} > 1 \end{cases} \quad \text{(S6)}$$

The diffusion coefficient[4] of liquid water is given as function of λ_w and temperatur

The water electro-osmotic drag effect is model by:[2]

$$q_{\mathrm{W,drag}} = n_{\mathrm{drag}} j/F \quad \text{(S7)}$$

where n_{drag} is the electroosmotic drag coefficient ($n_{\mathrm{drag}} = 2.5\lambda_w/22$)[2] and j is the operation current density,

The hydraulic permeation is calculated based on the liquid water pressure difference between the cathode and anode:[9]

$$q_{W,\mathrm{p}} = -\frac{k_w}{V_m} \nabla p \quad \text{(S8)}$$

where k_w is the membrane's permeability (5×10^{-20} m^2)[9] and p is the liquid water pressure.

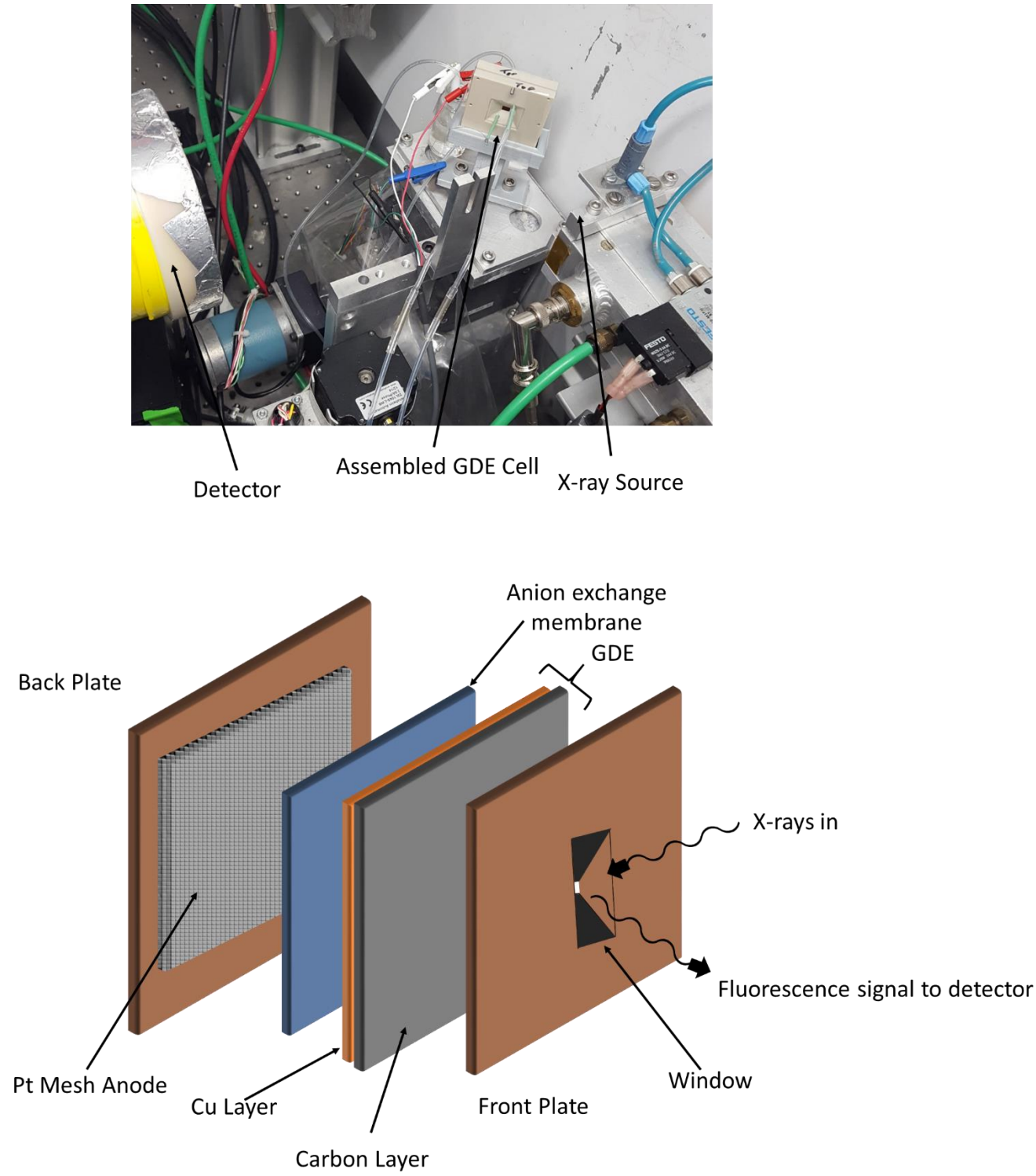

Figure S1. Assembled GDE cell in beamline 7-3 at SLAC (top). Expanded 3D view of the cell (bottom, not to scale).

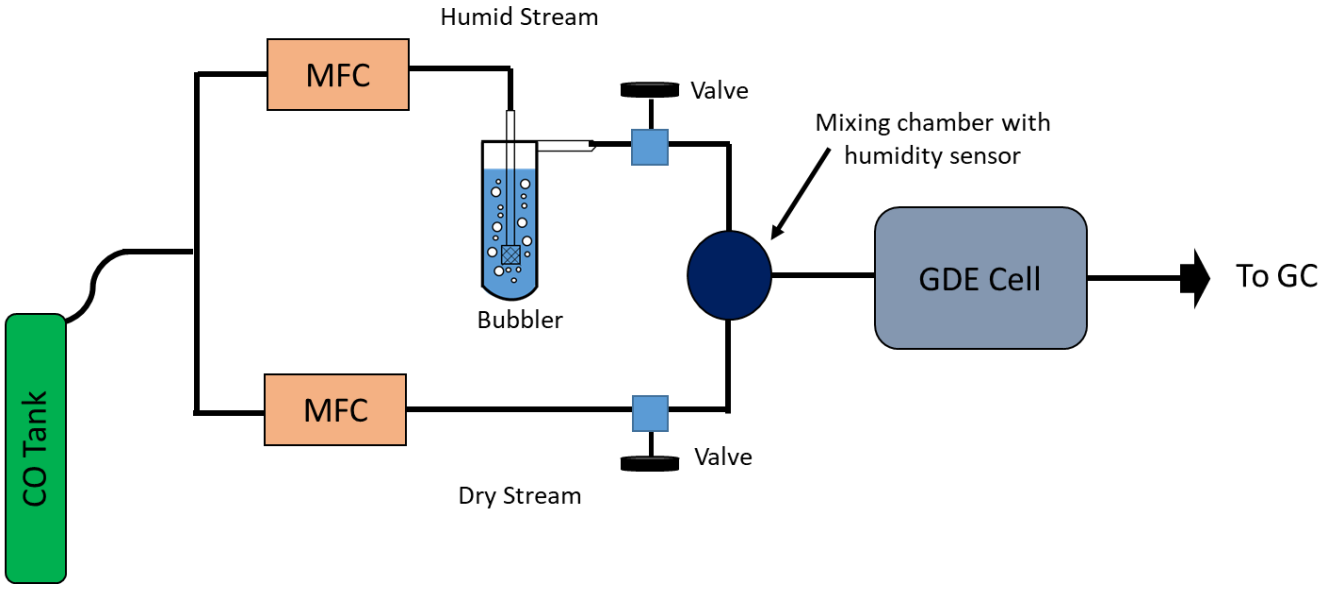

Figure S2. Schematic of the CORR experimental setup.

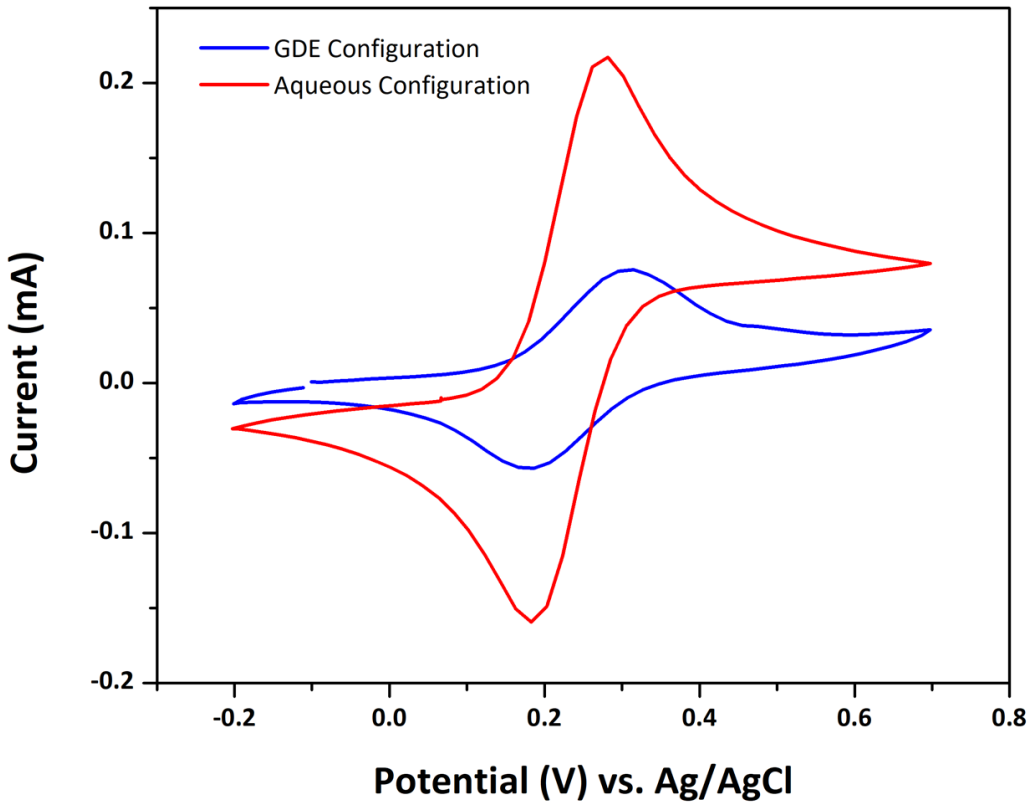

Figure S3. CV scans of 50 mM $K_3(FeCN_6)_3$ in 0.5 M KCl using a traditional aqueous configuration (red) and GDE configuration (blue). $E_{1/2}$ potential for the aqueous configuration is 0.2320 V and $E_{1/2}$ for the GDE configuration is 0.2506 V.

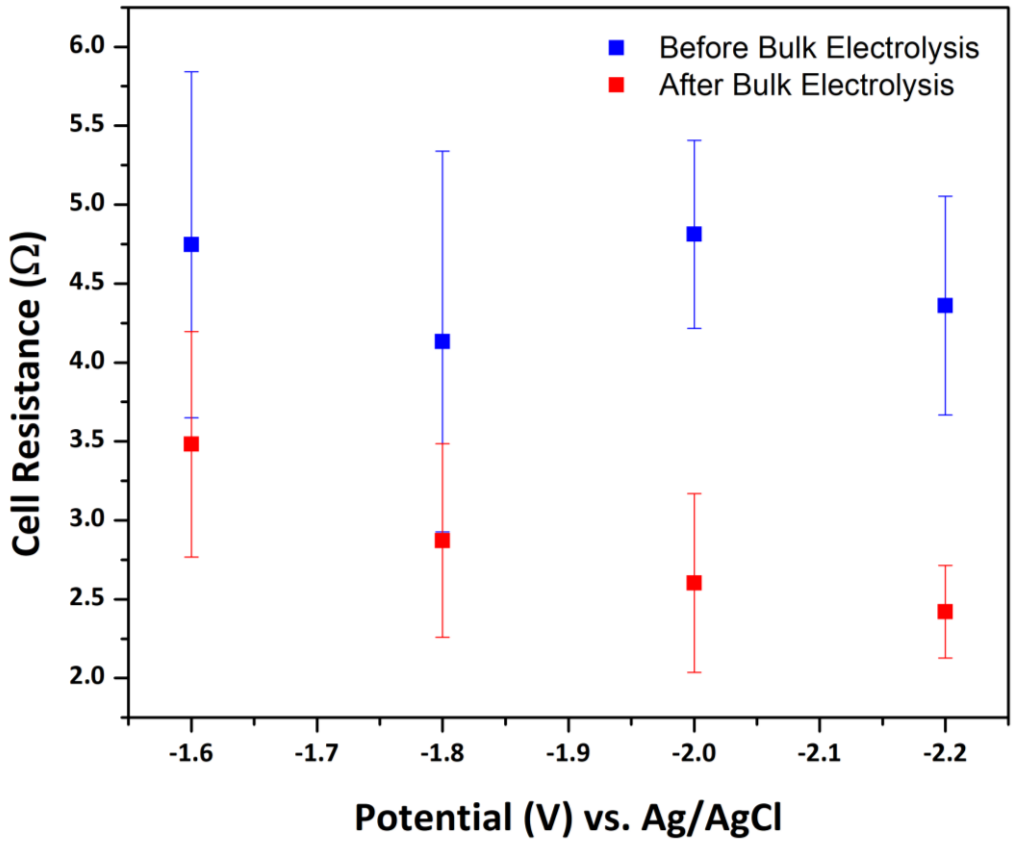

Figure S4. Cell resistance before (blue) and after (red) bulk electrolysis.

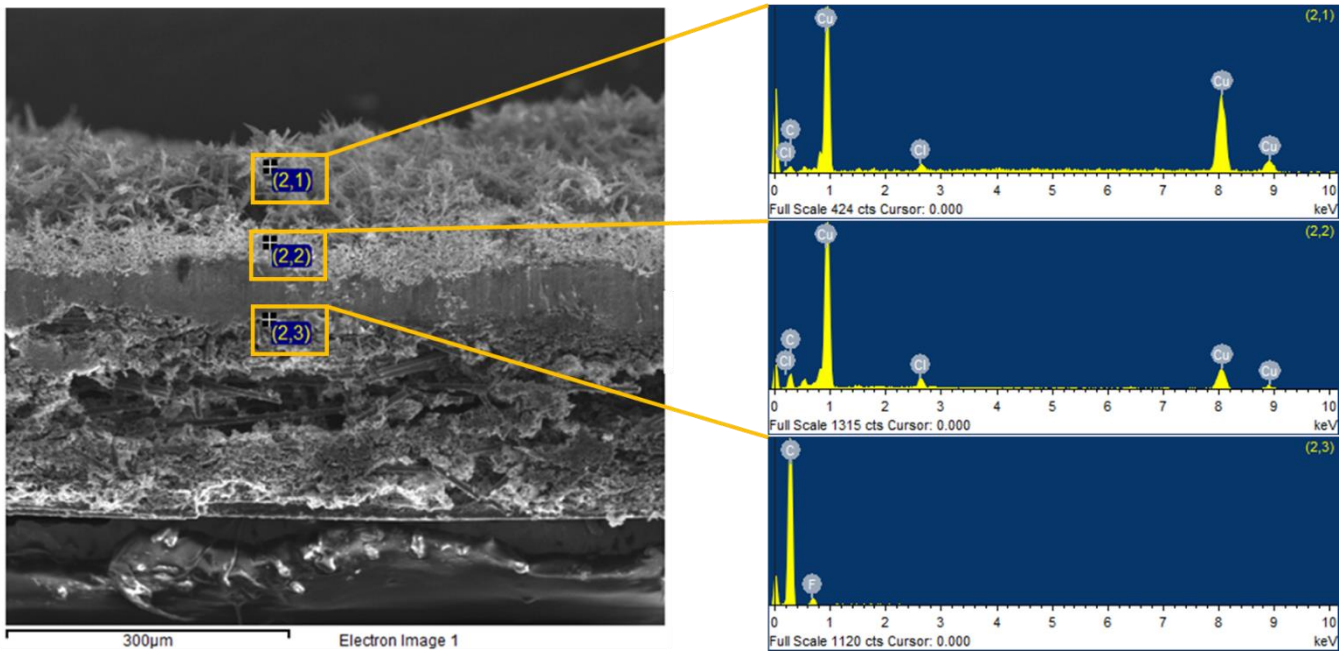

Figure S5. Cross sectional EDX mapping of the Cu-GDE indicating the Cu electrocatalyst layer, and C GDL layer.

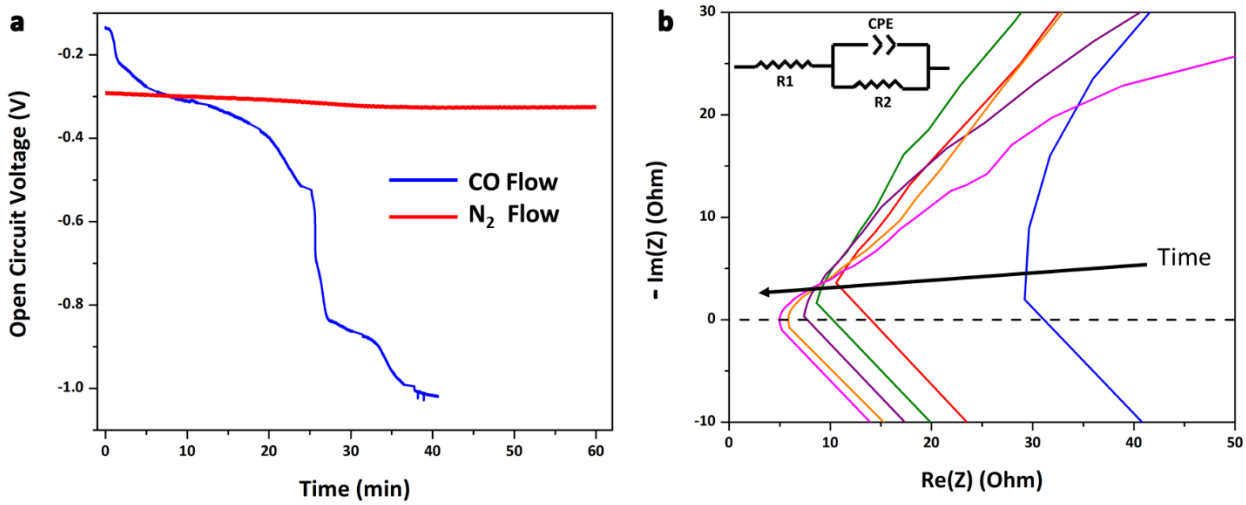

Figure S6. Typical OCV (a) and EIS (b) data for Cu-GDE under equilibration conditions.

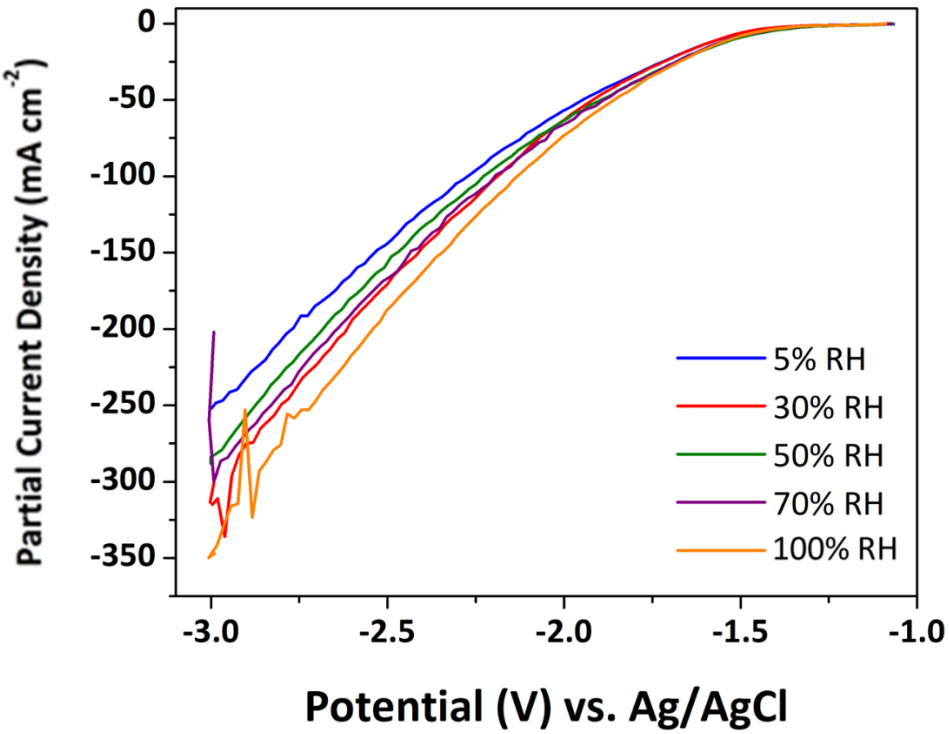

Figure S7. LSV scans of Cu-GDE at various relative humidity values.

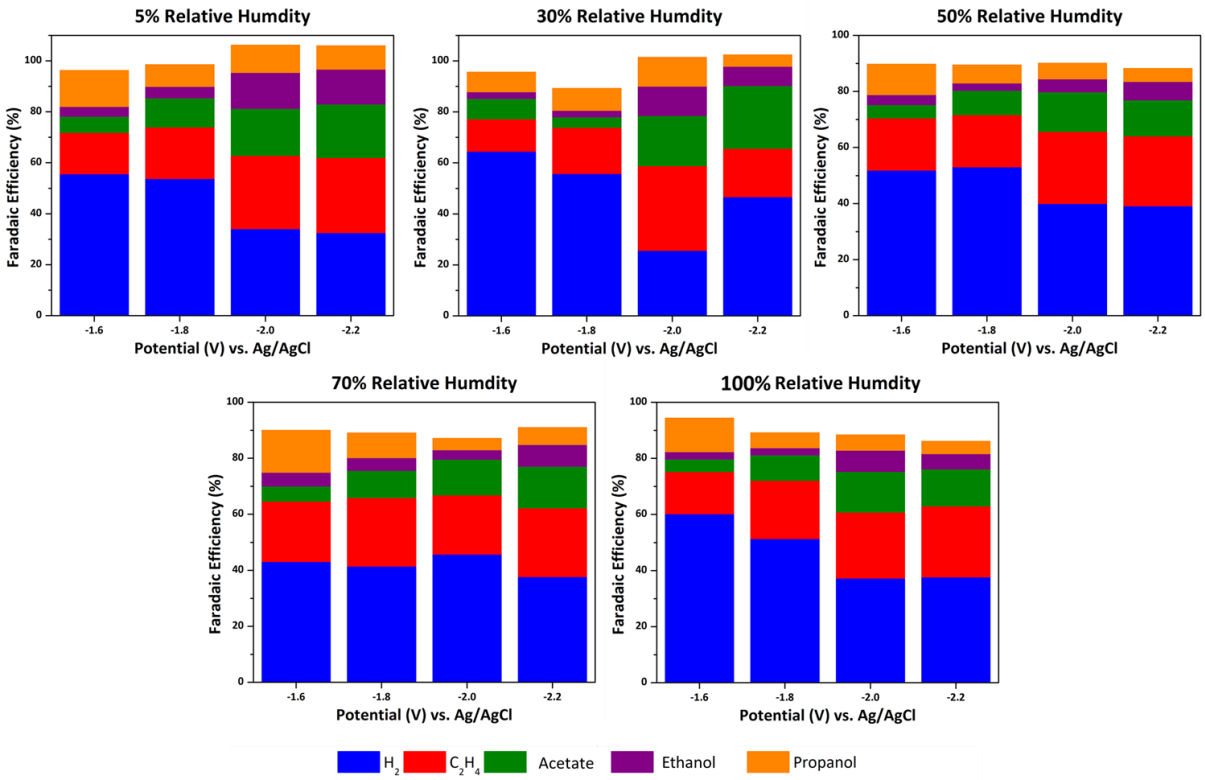

Figure S8. Product distributions as a function of applied potential and relative humidity (5% - 100%).

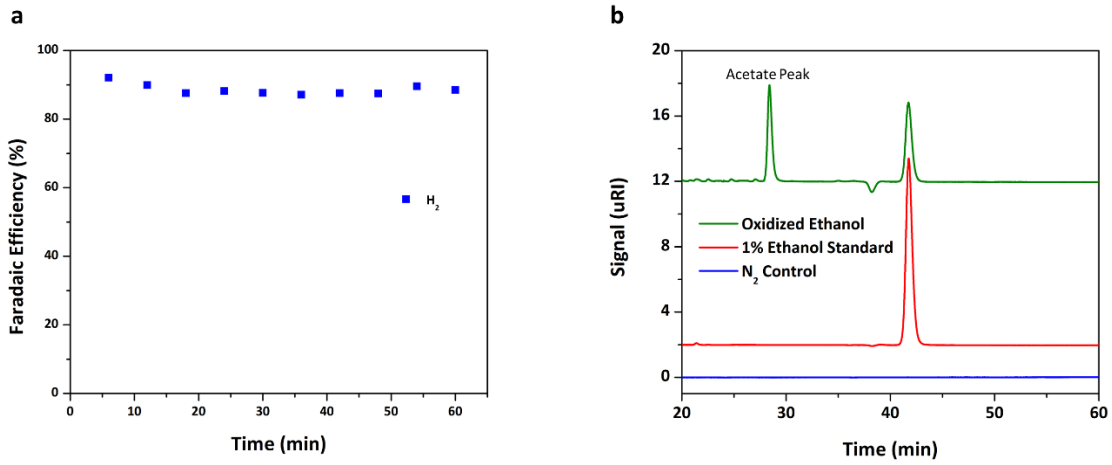

Figure S9. Gas product analysis from N_2 control experiments (a) and liquid product analysis (b) from N_2 control experiments and ethanol oxidation experiments.

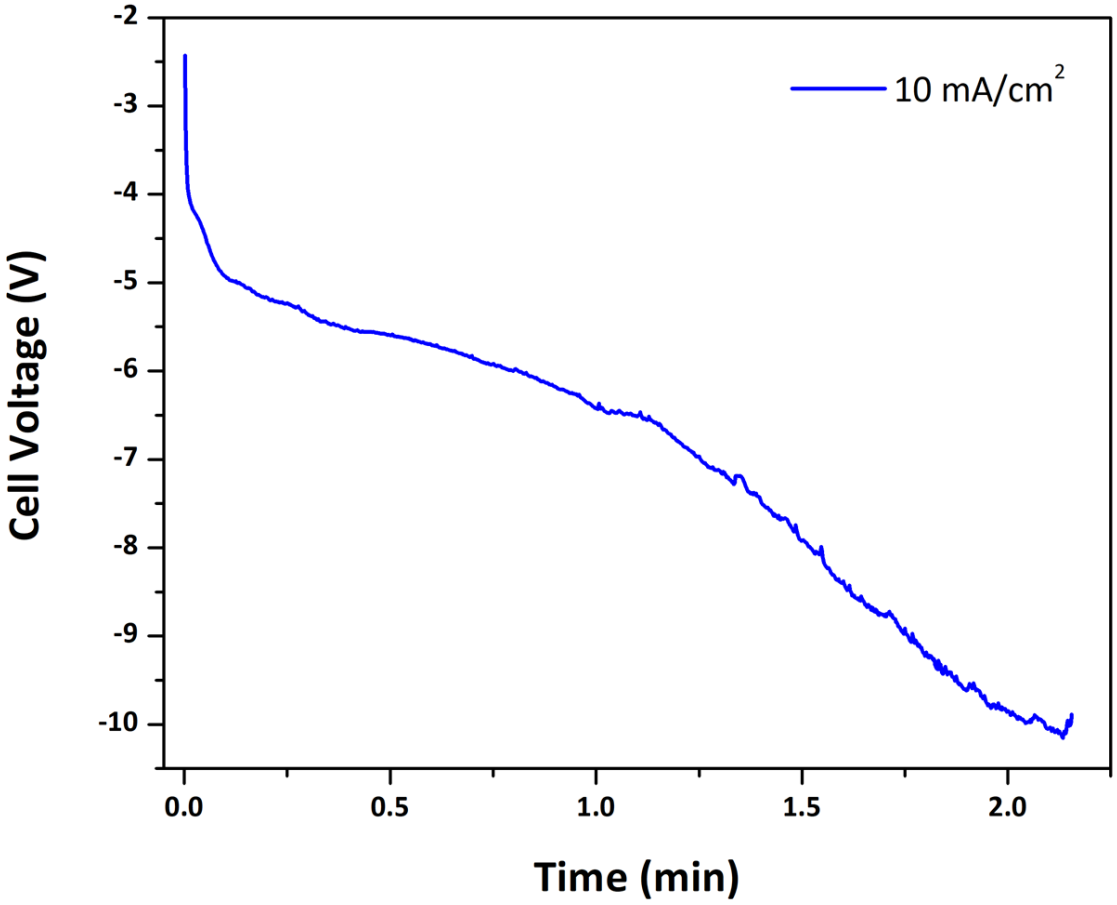

Figure S10. Cell voltage at 10 mA/cm^2 using an all vapor fed configuration.

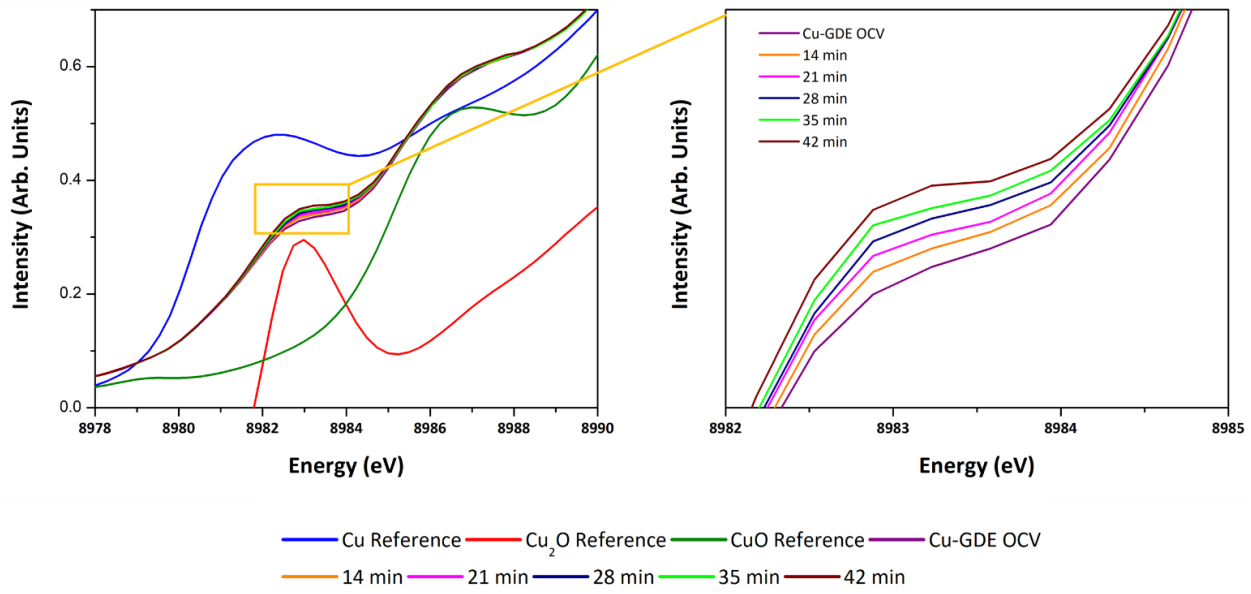

Figure S11. XANES measurements during OCV conditions where slight increase of the Cu_2O peak at ~8983 eV was observed.

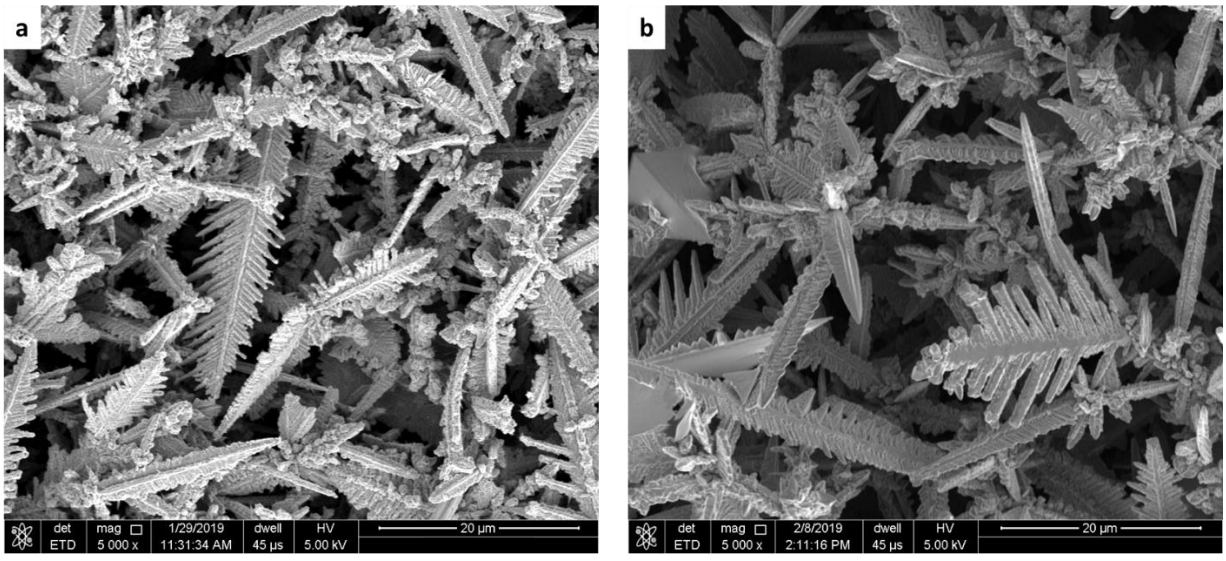

Figure S12. SEM images of Cu as deposited (a) and after bulk electrolysis (b).

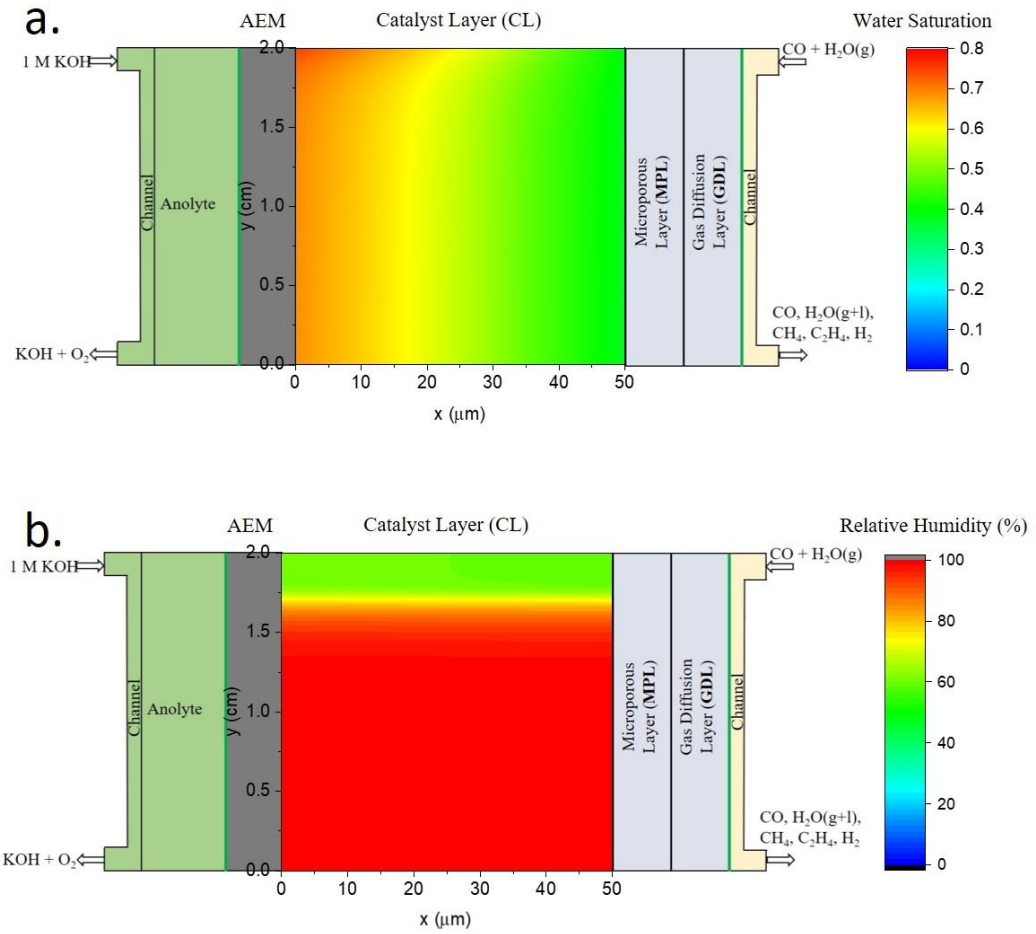

Figure S13. Contour plots of water saturation (a) and relative humidity (b) at catalyst layer with cathode inlet relative humidity of 50%.

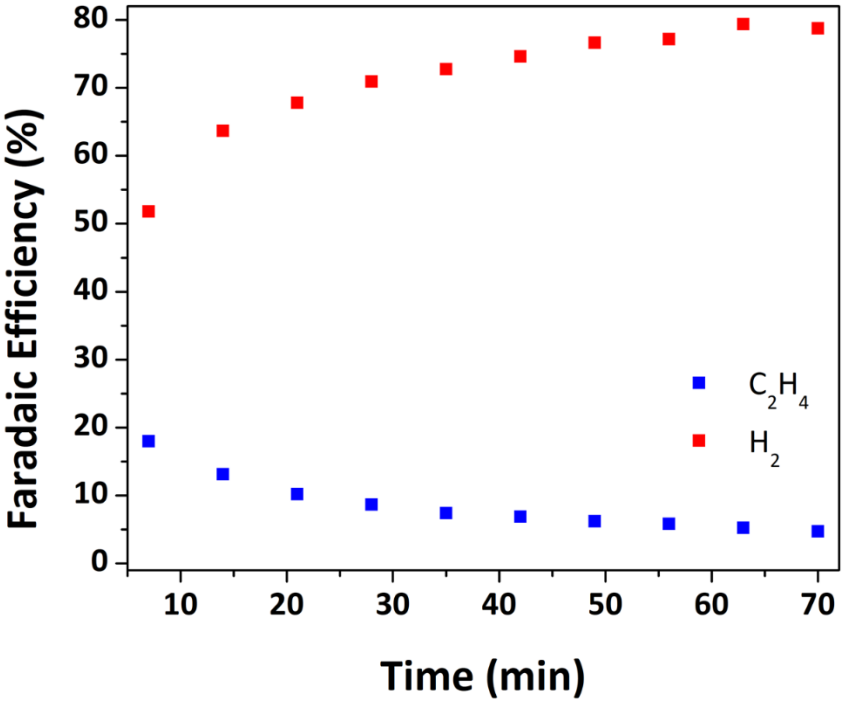

Figure S14. Faradaic yields of H_2 and C_2H_4 for an intentionally flooded GDE.

Table S2. Listed parameters for state-of-the-art devices for CO reduction. Potentials and current densities were selected based on the highest Faradaic efficiency reported.

Product	Faradaic Yield (%)	Current Density (mA cm^{-2})	Potential (V) vs RHE	Reference
C_2H_4	42	830	-0.72	10
	32	60	-1.43	11
	7	1.1	-0.45	12
	18.5	300	-0.72	13
	32.6	**87**	**-0.977**[a]	**This Work**
Ethanol	37	500	-0.32	10
	12	10	-1.43	11
	50	0.3	-0.3	12
	14	**52**	**-0.977**[a]	**This Work**
Acetate	30	500	-0.32	10
	30	35	2.36[b]	11
	20	0.02	-0.25	12
	24.6	**106**	**-1.177**[a]	**This Work**
Propanol	26	500	-0.42	10
	10	5	-1.35	11
	2	1.1	-0.45	12
	14.2	**5.5**	**-0.577**[a]	**This Work**
a) Converted from Ag/AgCl				
b) Total cell voltage				

References

1) Ravel, B.; Newville, M. ATHENA, ARTEMIS, HEPHAESTUS: data analysis for X-ray absorption spectroscopy using IFEFFIT. *J. Synchrotron Radiat.*, **2005**, 12, 537–541, DOI 10.1107/S0909049505012719.

2) J. Dujc, A. Forner-Cuenca, P. Marmet, M. Cochet, R. Vetter, J. O. Schumacher and P. Boillat. Modeling the effects of using gas diffusion layers with patterned wettability for advanced water management in proton exchange membrane fuel cells. *J. Electrochem. Energy Convers. Storage*, **2018**, 15, 021001-1–021001-14, DOI 10.1115/1.4038626.

3) Gostick, J.T.; Ioannidis, M.A.; Fowler, M.W.; Pritzker, M.D. Wettability and capillary behavior of fibrous gas diffusion media for polymer electrolyte membrane fuel cells. *J. Power Source*s, **2009**, 194, 433–444, DOI 10.1016/j.jpowsour.2009.04.052.

4) Wu, H.; Li, X.; Berg, P. On the modeling of water transport in polymer electrolyte membrane fuel cells. *Electrochim. Acta*, **2009**, 54, 6913–6927, DOI 10.1016/j.electacta.2009.06.070.

5) Vetter, R.; Schumacher, J.O. Free open reference implementation of a two-phase PEM fuel cell model. *Comput. Phys. Commun.*, **2019**, 234, 223–234, DOI 10.1016/j.cpc.2018.07.023.

6) Weng, L.C.; Bell, A.T; Weber, A.Z. Modeling gas-diffusion electrodes for CO_2 reduction. *Phys. Chem. Chem. Phys.*, **2018**, 20, 16973–16984, DOI 10.1039/C8CP01319E.

7) Li, Q.; Gong, J.; Peng, S.; Lu, S.; Sui, P.C.; Djilali, N.; Xiang, Y. Theoretical design strategies of bipolar membrane fuel cell withenhanced self-humidification behavior. *J. Power Sources*, **2016**, 307, 358–367, DOI 10.1016/j.jpowsour.2016.01.016.

8) Qin, C.; Rensink, D.; Fell, S.; Hassanizadeh, S.; Two-phase flow modeling for the cathode side of a Polymer electrolyte fuel cell. *J. Power Sources*, **2012**, 197, 136–144, DOI 10.1016/j.jpowsour.2011.08.095.

9) Zawodzinski, T.A; Davey, J.; Valerio, J.; Gottesfeld, S. The water content dependence of electro-osmotic drag in proton-conducting polymer electrolytes. *Electrochim. Acta*, **1995**, 40, 297–302, DOI 10.1016/0013-4686(94)00277-8.

10) Jouny, M.; Luc, W.; Jiao, F. High-Rate Electroreduction of Carbon Monoxide to Multi-Carbon Products. *Nat. Catal.* **2018**, *1*, 748–755, DOI 10.1038/s41929-018-0133-2.

11) Ripatti, D. S.; Veltman, T. R.; Kanan, M. W. Carbon Monoxide Gas Diffusion Electrolysis That Produces Concentrated C_2 Products with High Single-Pass Conversion. *Joule* **2019**, *3*, 240–256, DOI 10.1016/j.joule.2018.10.007.

12) Raciti, D.; Cao, L.; Livi, K. J. T.; Rottmann, P. F.; Tang, X.; Li, C.; Hicks, Z.; Bowen, K. H.; Hemker, K. J.; Mueller, T.; et al. Low-Overpotential Electroreduction of Carbon Monoxide Using Copper Nanowires. *ACS Catal.* **2017**, *7*, 4467–4472, DOI 10.1021/acscatal.7b01124.

13) Han, L.; Zhou, W.; Xiang, C. High-Rate Electrochemical Reduction of Carbon Monoxide to Ethylene Using Cu-Nanoparticle-Based Gas Diffusion Electrodes. *ACS Energy Lett.* **2018**, *3*, 855–860, DOI 10.1021/acsenergylett.8b00164.